

Nuclear Astrophysics

K. Langanke^{a *}

^aInstitute for Physics and Astronomy, University of Aarhus, DK-8000 Aarhus C, Denmark

The manuscript reviews progress achieved in recent years in various aspects of nuclear astrophysics, including stellar nucleosynthesis, nuclear aspects of supernova collapse and explosion, neutrino-induced reactions and their possible role in the supernova mechanism and nucleosynthesis, explosive hydrogen burning in binary systems, and finally the observation of γ -rays from supernova remnants.

1. Introduction

In recent years nuclear astrophysics has grown into one of the major subfields in nuclear physics and has become motivation for many on-going and future developments worldwide. This is partly related to the fact that the interest within nuclear astrophysics has also shifted in the last years. Has the focus been in the past on the understanding of hydrostatic burning in stars and related stellar evolution involving mainly nuclear physics along the valley of stability (for a delightful reference the reader is referred to Willy Fowler's Nobel lecture [1]), interest has shifted to astrophysical sites and scenarios which require knowledge of nuclear processes and properties at the two extreme sides of the nuclear chart, very proton- and neutronrich nuclei. Clearly progress in these domains and hence more reliable simulations of the astrophysical scenarios is expected from radioactive ion beam (RIB) facilities and this is exactly the reason why the (nuclear) astrophysics community so strongly supports the RIB initiatives worldwide.

Important progress has been achieved in many aspects of nuclear astrophysics. Due to new observational tools (e.g. Hubble Space Telescope, COBE, ROSAT, Superkamiokande) astronomical observations of the universe and its contents cover now the different wavelengths of the electromagnetic spectrum and detect particles and with increasing importance also γ -rays which allow to draw conclusions about the nuclear processes involved. Besides the various RIB initiatives, improvements in laboratory nuclear astrophysics has also been made possible by new detector developments as well as by moving underground. For example, the LUNA collaboration, working in the Gran Sasso underground laboratory, succeeded at measuring, for the first time, one of the reactions in the pp-chain at those energies at which it proceeds most effectively in our sun. Finally, progress in computer hard- and software going hand in hand with improved nuclear and astrophysical models has contributed to more realistic and better simulations and understanding of

*The work was partly supported by the Danish Research Council.

various astrophysical scenarios, but have also raised new questions which will keep the field exciting and vivid in the coming years.

This review will attempt to present some of the highlights of the recent years, but given the width of the field it cannot be complete (for references to subjects not discussed here see the NUPECC report on Nuclear and Particle Astrophysics [2]). As a red thread we will focus mainly on the nuclear physics related to the understanding of type II supernovae including relevant nuclear input for the collapse, the explosion mechanism and related nucleosynthesis processes. Special attention will be paid to the role played by neutrinos. Finally we will briefly discuss explosive hydrogen burning in novae and x-ray bursters. But at the beginning we like to report about the first successful studies of the chemical evolution of a galaxy resembling our Milky Way.

2. Galactical chemical evolution

The general ideas of the synthesis of elements in the universe has been derived now more than 40 years ago by Burbidge, Burbidge, Fowler and Hoyle [3] and, independently, by Cameron [4]. Due to this picture, the light elements (mainly hydrogen and helium) have been made during the Big Bang, while the breeding places for most of the other elements are stars. The stars generate the energy, which allows them to stabilize and shine for millions of years and longer, by transmuting nuclear species, thus forming new elements. These processes occur inside the star, but are eventually released if the star for example is massive enough and finally explodes in a type II supernova. The freshly bred nuclear material is mixed into the interstellar medium (ISM) and can thus become part of the initial abundance composition for a new star to be formed. Thus the galactical chemical evolution represents a ‘cosmic cycle’, and the modellation of the observed solar abundances (e.g. [5]) requires the simulations of the formation of a galaxy and of the stellar mass distribution, birth rates, evolution and lifetimes. Importantly one has to calculate the abundances produced by a star of a given mass and the amount and composition of matter ejected into the ISM by the star’s final type II supernova explosion. Finally contributions of type Ia supernovae have to be added which involve the formation and evolution of binary systems composed of a giant star with a hydrogen envelope and an accreting white dwarf.

Despite its complexity, rather consistent studies of the galactical chemical evolution have been performed by Woosley and collaborators [6] and by Nomoto, Thielemann and collaborators [7]. Although the simulations involve still a few model assumptions (from the nuclear input, the rate of the important $^{12}\text{C}(\alpha, \gamma)^{16}\text{O}$ reaction is still too uncertain [8]), excellent agreement is obtained with solar abundances [9] for 76 isotopes from hydrogen to zinc, when the calculation is sampled at a time $4.55 \cdot 10^9$ years ago at a distance of 8.5 kpc from the galaxy center (corresponding to birth time and position of our sun in the Milky Way). As can be seen in Fig. 1, most of the abundances agree within a factor of 2.

It should be mentioned that specific nuclei appear to be almost entirely (e.g. ^{11}B , ^{19}F) or in a large fraction (e.g. ^{10}B , ^{15}N) made by neutrino nucleosynthesis [10]. These nuclei are the product of reaction sequences induced by neutral current (ν, ν') reactions on very abundant nuclei like ^{12}C , ^{16}O and ^{20}Ne , when the flux of neutrinos generated by cooling of the neutron star passes through the overlying shells of heavy elements.

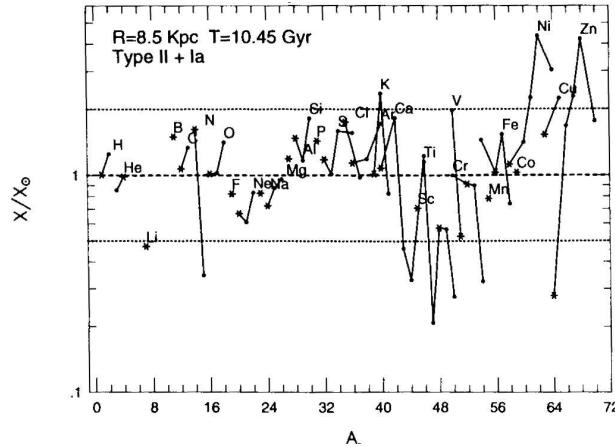


Figure 1. Ratio of the calculated and observed solar abundances for stable isotopes from hydrogen to zinc. The dotted lines mark deviations by a factor of 2 between calculation and observation. (from [6])

3. Nuclear physics input in supernovae

At the end of hydrostatic burning, a massive star consists of concentric shells that are the remnants of its previous burning phases (hydrogen, helium, carbon, neon, oxygen, silicon). Iron is the final stage of nuclear fusion in hydrostatic burning, as the synthesis of any heavier element from lighter elements does not release energy; rather, energy must be used up. If the iron core, formed in the center of the massive star, exceeds the Chandrasekhar mass limit of about 1.44 solar masses, electron degeneracy pressure cannot longer stabilize the core and it collapses starting what is called a type II supernova. In its aftermath the star explodes and parts of the iron core and the outer shells are ejected into the ISM. Although this general picture has been confirmed by the various observations from supernova SN1987a, simulations of the core collapse and the explosion are still far from being completely understood and robustly modelled. In the following subsections we will briefly review some recent progress, related to nuclear input, which might help for more reliable supernova simulations.

3.1. Weak interaction rates for the core collapse

As pointed out by Bethe *et al.* [11,12] the collapse is very sensitive to the entropy and to the number of leptons per baryon, Y_e . In turn these two quantities are mainly determined by weak interaction processes, electron capture and β decay. First, in the early stage of the collapse Y_e is reduced as electrons are captured by Fe-peak nuclei. This reduces the electron pressure, thus accelerating the collapse, and shifts the distribution of nuclei present in the core to more neutron-rich material. Second, many of the nuclei present can also β decay. While this process is quite unimportant compared to electron capture for initial Y_e values around 0.5, it becomes increasingly competitive for neutron-rich nuclei

due to an increase in phase space related to larger Q_β values.

Knowing the importance of the weak interaction process, Fuller *et al.* (usually called FFN) have systematically estimated the rates for nuclei in the mass range $A = 45 - 60$ putting special emphasis on the importance of electron capture to the Gamow-Teller (GT) giant resonance [13]. Another important idea in FFN was to recognize the role played by the GT resonance in β decay. Other than in the laboratory, β decay under stellar conditions are significantly increased due to thermal population of the GT back resonance in the parent nucleus (the GT back resonance are the states reached by the strong GT transitions in the inverse process (electron capture) built on the ground and excited states [13,14]) allowing for a transition with a large nuclear matrix element and increased phase space. Indeed, Fuller et al. concluded that the β decay rates under collapse conditions are dominated by the decay of the back resonance.

The GT contribution to the electron capture and β decay rates has been parametrized by FFN on the basis of the independent particle model. To complete the FFN rate estimate, the GT contribution has been supplemented by a contribution simulating low-lying transitions. Recently the FFN rates have been updated and extended to heavier nuclei by Aufderheide *et al.* [14].

In recent years, however, the parametrization of the GT contribution, as adopted in [13, 14], has become questionable when experimental information about the GT distribution in nuclei became available. These data clearly indicate that the GT strength is not only quenched, but also fragmented over several states at modest excitation energies in the daughter nucleus [15–19]. Thus the need for an improved theoretical description has soon been realized [20–22], but it became also apparent that a reliable reproduction of the GT distribution in nuclei requires large shell model calculations which account for all correlations among the valence nucleons in a major oscillator shell. Such $0\hbar\omega$ shell model calculations are now possible and they come in two varieties: large-scale diagonalization approaches [23] and shell model Monte Carlo (SMMC) techniques [24,25]. The latter can treat the even larger model spaces, but has limitations in its applicability to odd- A and odd-odd nuclei at low temperatures, which does not apply to the former. More importantly the diagonalization approach allows for detailed spectroscopy, while the SMMC model yields only an “averaged” GT strength distribution which introduces some inaccuracy into the calculation of the capture and decay rates.

Core collapse electron capture and β decay rates have now been calculated for the relevant nuclei in the mass range $A = 46 - 65$ [27]. The calculations have been performed by shell model diagonalization in model spaces large enough (involving typically 10 million or more configurations) to guarantee that the GT strength distribution is virtually converged. Adopting a recently developed, improved version of the KB3 interaction [28] these calculations reproduce all measured GT strength distributions very well (after scaling by the universal factor, $(0.74)^2$ [31,30,32]) and describe the experimental level spectrum of the nuclei involved quite accurately [29]. Fig. 2 compares the measured and calculated GT distributions for several nuclei in the mass range $A = 50 - 64$. Furthermore modern large-scale shell model calculations also agree with measured half-lives very well. Thus for the first time one has a tool in hand which allows for a reliable calculation of presupernova electron capture and β decay rates.

Data and shell model calculations indicate systematic differences in the location of the

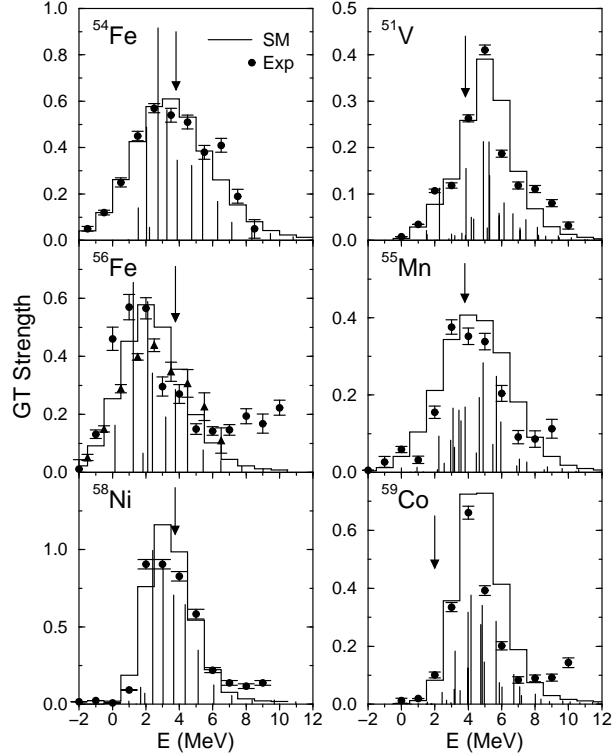


Figure 2. Comparison of the shell model GT strength distribution (histogram) with data [15–19] for selected even-even (right) and odd-A nuclei (left). For the comparison the calculated discrete spectrum has been folded with the experimental resolution. The positions of the GT centroid assumed in the FFN parametrization are shown by arrows.

main GT resonance strength compared to the parametrization of FFN [26,27]. In capture on even-even nuclei the GT strength resides at lower excitation energies in the daughter than assumed by FFN, while in odd-A and odd-odd nuclei the GT strength is centered at higher excitation energies. As a consequence, the shell model electron capture rates on odd-A and odd-odd nuclei are significantly (by an order of magnitude or more) smaller than the compiled rates, while the capture rates on even-even nuclei are approximately the same, as FFN had often intuitively compensated the smaller GT contribution (compared with the shell model) by the empirically added low-lying transition strength. Which consequences do the misplacement of the GT centroids have for the competing β decays? In odd-A and even-even nuclei (the daughters of electron capture on odd-odd nuclei), experimental data and shell model studies place the back-resonance at higher excitation energies than assumed by FFN and Aufderheide et al. [14]. Correspondingly, its population becomes less likely at the temperatures available during the early stage of the collapse ($T_9 \approx 5$, where T_9 measures the temperature in 10^9 K) and hence the contribution of the back-resonance to the β decay rates for even-even and odd-A nuclei decreases.

In contrast, the shell model β decay rate for odd-odd nuclei often are slightly larger than the FFN rates, as for these nuclei, all available data, stemming from (n,p) reaction cross section measurements on even-even nuclei like $^{54,56,58}\text{Fe}$ or $^{58,60,62,64}\text{Ni}$, and all shell model calculations indicate that the back-resonance resides actually at lower excitation energies than previously parametrized.

What might the revised electron capture and β decay rates mean for the core collapse? One can investigate this question by studying the change of the electron-to-baryon ratio, Y_e , along a stellar trajectory as given in Ref. [14]. As can be seen in Fig. 3, the shell model rates reduce Y_e^{ec} significantly compared with the FFN; by more than an order of magnitude for $Y_e < 0.47$. This is due to the fact, that, except for ^{56}Ni , all shell model electron capture rates are smaller than the recommendations given in the FFN compilations [13]. The shell model β decay rates also reduce \dot{Y}_e^β , however, by a smaller amount than for electron capture. This is mainly caused by the fact that the shell model β decay rates of odd-odd nuclei are about the same as the FFN rates or even slightly larger, for reasons discussed above. The important feature in Fig. 3 is that β decay rates are larger than the electron capture rates for $Y_e = 0.42 - 0.455$, which is also already true for the FFN rates. This, however, had apparently not been considered in collapse calculations yet which used quite outdated β decay rates [33].

The consequences of the shell model rates on the core collapse has to be explored by detailed and consistent calculations. One expects that in the early stage of the collapse the stellar trajectory is, for a given density, at a higher temperature, as, due to the slower electron capture rates, the star radiates less energy away in form of neutrinos until $Y_e = 0.455$ is reached, and the β decay rates become larger than the electron rates. This might lead to cooler cores and larger Y_e values at the formation of the homologous core, as pointed out in [33].

4. Towards a robust supernova explosion

Electron capture, β decay and photodisintegration cost the core energy and reduce its electron density. As a consequence, the collapse is accelerated. An important change in the physics of the collapse occurs, if the density reaches $\rho_{\text{trap}} \approx 4 \cdot 10^{11} \text{ g/cm}^3$. Then neutrinos are essentially trapped in the core, as their diffusion time (due to coherent elastic scattering on nuclei) becomes larger than the collapse time. After neutrino trapping, no energy is carried away from the core. Shortly after (at $\rho \approx 10^{12} \text{ g/cm}^3$), neutrinos are thermalized by inelastic scattering on electrons. Then all reactions are in equilibrium, including the weak processes discussed above. The degeneracy of the (trapped) neutrino Fermi gas hinders a complete neutronization. As a consequence, Y_e remains rather large through the collapse ($Y_e = 0.35 - 0.38$ [12], possible consequences due the modified weak interaction rates have to be explored). To balance the charge, the number of protons must therefore also be large and this can only be achieved in heavy nuclei. The collapse has a rather large order and the entropy stays small during the collapse [11].

After neutrino trapping, the collapse proceeds homologously [35], until nuclear densities ($\rho_N \approx 10^{14} \text{ g/cm}^3$) are reached. As nuclear matter has a finite compressibility, the homologous core decelerates and bounces in response to the increased nuclear matter pressure; this eventually drives an outgoing shock wave into the outer core; i.e. the envelope of

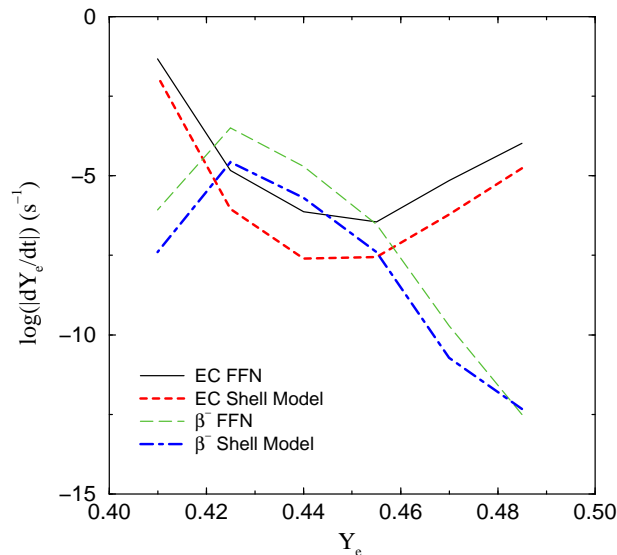


Figure 3. Change in the total electron capture and β decay rates, \dot{Y}_e^{ec} and \dot{Y}_e^β , respectively. The shell model results are compared with the FFN results [13] along the same stellar trajectory as in Fig. 14 of Ref. [14].

the iron core outside the homologous core, which in the meantime has continued to fall inwards at supersonic speed. The core bounce with the formation of a shock wave is believed to be the mechanism that triggers a supernova explosion, but several ingredients of this physically appealing picture and the actual mechanism of a supernova explosion are still uncertain and controversial. If the shock wave is strong enough not only to stop the collapse, but also to explode the outer burning shells of the star, one speaks about the ‘prompt mechanism’. However, it appears as if the energy available to the shock is not sufficient, and the shock will store its energy in the outer core, for example, by excitation of nuclei.

After the supernova has exploded, a compact remnant with a gravitational mass of order one solar mass is left behind; this mass is slightly increased to 1.3-1.5 solar masses in the first second after the bounce by accretion. The remnant is very lepton rich (electrons and neutrinos), the latter being trapped as their mean free paths in the dense matter is significantly shorter than the radius of the neutron star. It takes a fraction of a second [36] for the trapped neutrinos to diffuse out, giving most of their energy to the neutron star during that process and heating it up. The cooling of the protoneutron star then proceeds by pair production of neutrinos of all three generations which diffuse out. After several tens of seconds the star becomes transparent to neutrinos and the neutrino luminosity drops significantly [37]. In the ‘delayed mechanism’, the shock wave can be revived by these outward diffusing neutrinos, which carry most of the energy set free in the gravitational collapse of the core. The delayed mechanism has been discovered by

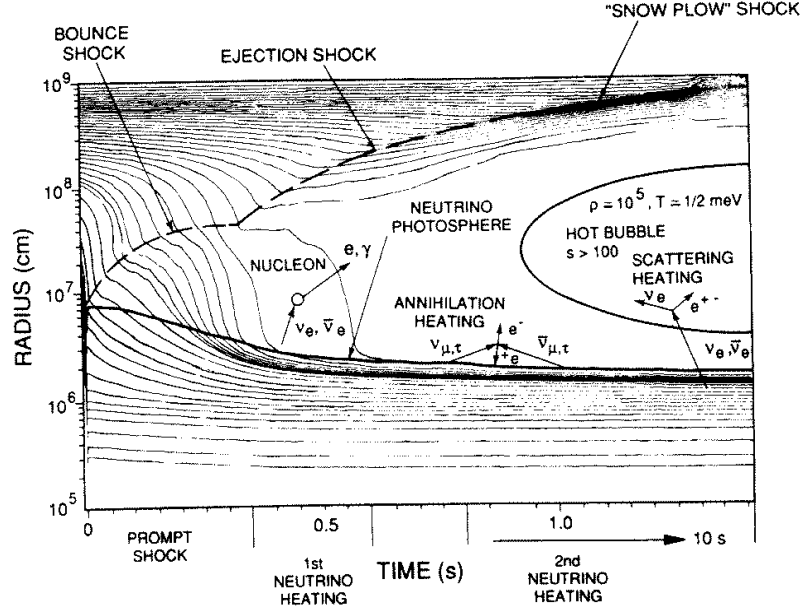


Figure 4. Mass trajectories during a core collapse leading to the discovery of the delayed explosion mechanism by Wilson. The bounce occurs at time $t = 0$. The shock travels outwards for a short time, gets stalled and is later revived by the neutrinos generated due to cooling of the nascent neutron star. Above the neutron star forms the radiation bubble which might be the site for the nuclear r-process. (from [34]).

Wilson [38]; the mass trajectories of his computer simulation are shown as function of time after the bounce in Fig. 4.

Although the details of the neutrino distributions leaving the protoneutron star are still subject of research, it is generally accepted that there is a temperature hierarchy between the various neutrino types introduced by the charged current reactions with the surrounding neutron-rich matter. Thus, μ and τ neutrinos and their antiparticles (usually combiningly referred to as ν_x neutrinos) have the distribution with the highest temperature ($T = 8$ MeV if one accepts a Fermi-Dirac distribution with zero chemical potential [10]). All ν_x neutrinos have the same distribution and thus potential oscillations between these neutrino types as suggested by the Superkamiokande results on atmospheric neutrinos [39] are not important for the topics discussed below. As the ν_e and $\bar{\nu}_e$ neutrinos interact with the neutron-rich matter via $\nu_e + n \rightarrow p + e^-$ and $\bar{\nu}_e + p \rightarrow n + e^+$, the $\bar{\nu}_e$ neutrinos have a higher temperature ($T \approx 5.6$ MeV) than the ν_e neutrinos ($T = 4$ MeV). It is useful for the following discussions to note that these temperatures correspond to average neutrino energies of $\bar{E}_\nu = 25$ MeV for ν_x neutrinos, while $\bar{E}_\nu = 16$ MeV and 11 MeV for $\bar{\nu}_e$ and ν_e neutrinos.

In the delayed supernova mechanism, neutrinos deposit energy in the layers between

the nascent neutron star and the stalled prompt shock. This lasts for a few 100 ms, and requires about 1% of the neutrino energy to be converted into nuclear kinetic energy. The energy deposition increases the pressure behind the shock and the respective layers begin to expand, leaving between shock front and neutron star surface a region of low density, but rather high temperature. This region is called the ‘hot neutrino bubble’ and, as we will discuss below, might be the site of the nuclear r-process. The persistent energy input by neutrinos keeps the pressure high in this region and drives the shock outwards again, eventually leading to a supernova explosion.

It has been found that the delayed supernova mechanism is quite sensitive to physics details deciding about success or failure in the simulation of the explosion. Very recently, two quite distinct improvements have been proposed which should make the explosion mechanism more robust, as they increase the efficiency of the energy transport to the stalled shock.

4.1. Convection

Two-dimensional [40] and three-dimensional [41] hydrodynamic simulations have recently become possible and have clearly demonstrated the existence of convective instabilities inside the protoneutron star. The convective velocities can even reach the local sound speed, generating strong pressure waves by the convective flow [42]. Near the protoneutron star surface the convective mixing is accompanied by an increase of the neutrino luminosities during the early phase of the explosion; the effect can be seen by comparing models B1 and B2 in Fig. 5. Due to the rather violent convection, neutrinos are transported out of the dense interior of the protoneutron star much faster than by diffusion, making the revival of the shock more efficient.

4.2. Neutrino opacities in dense matter

Numerical simulations have also found convective instabilities in the ‘hot neutrino bubble’ region [44–47]. However, a realistic description for this region requires an adequate treatment of the neutrino transport and opacities in dense matter. For a long time, this subject has received rather little attention, but within the last year it has evolved into a vividly studied subject.

To describe charged- and neutral-current reactions of neutrinos in nuclear matter, one has to know the response of the system usually characterized by dynamic form factors $S(q_0, q)$, where q_0 is the energy transfer to the baryons and q the momentum transfer. At the mean field level, the function S can be evaluated exactly if the single particle dispersion relation is known [48]. Compared to the case of a non-interacting system, strong interaction corrections are incorporated by adopting an effective mass parameter, which, like the single particle potentials, are chosen as density dependent [48].

However, nucleon-nucleon correlations introduced by the residual interaction (for which, for example, a Migdal parametrization like in Fermi-liquid theory can be adopted, potentially extended by a tensor component [51–53]) turn out to be quite important [50,51]. For example, these effects can be studied within the random phase approximation. Then, neutral current reactions are sensitive to the density-density and spin-density response functions of nuclear matter, while charged current reactions depend on the isospin density and spin-isospin density response functions [51].

For neutral-current reactions like neutrino-neutron scattering, it is found that the re-

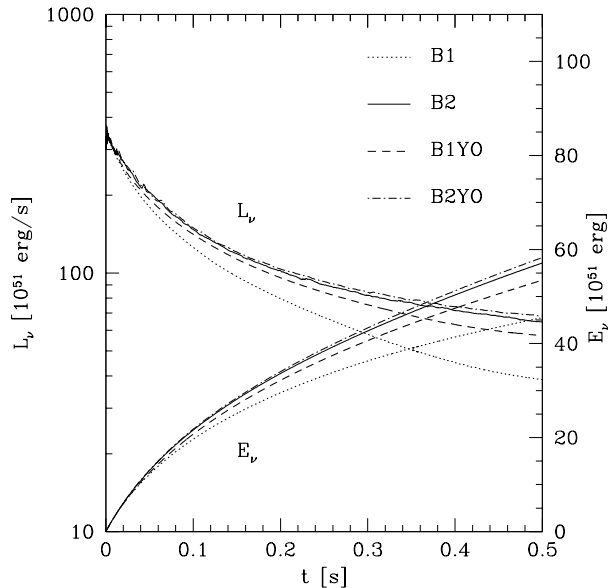


Figure 5. Total surface neutrino luminosity L_ν and integrated energy emission E_ν as functions of time for models without (B1) and with (B2) convection and with standard neutrino opacities (B1YO) and reduced neutrino opacities (B2YO) (courtesy of H.-T. Janka, [43]).

pulsive interaction shifts strength to larger q_0 enhancing the collective excitations, while the cross sections are significantly reduced at small energy transfers q_0 , as is demonstrated in Fig. 6 for pure neutron matter. The same effects are observed in charged-current reactions, where the excitation of the Gamow-Teller and giant dipole resonances take away strength from low q_0 .

It appears that nucleon-nucleon correlations reduce the neutrino opacities in dense nuclear matter considerably compared with the free gas estimate [50,51]. This might imply shorter time scales for the deleptonization and cooling of the protoneutron star and a more efficient energy transport to the stalled shock (see also the models B1YO and B2YO in Fig. 5).

5. R-process in the hot neutrino bubble

Within the last few years the neutrino-driven wind model has been widely discussed as the possible site of r-process nucleosynthesis [54,55]. Here it is assumed that the r-process occurs in the layers heated by neutrino emission and evaporating from the hot protoneutron star after core collapse. In this model (e.g. [56]), a hot blob of matter with entropy per baryon S_b and electron-to-baryon ratio Y_e , initially consisting of neutrons, protons and α -particles in nuclear statistical equilibrium (NSE), expands adiabatically and cools. Nucleons and nuclei combine to heavier nuclei, with some neutrons and α -

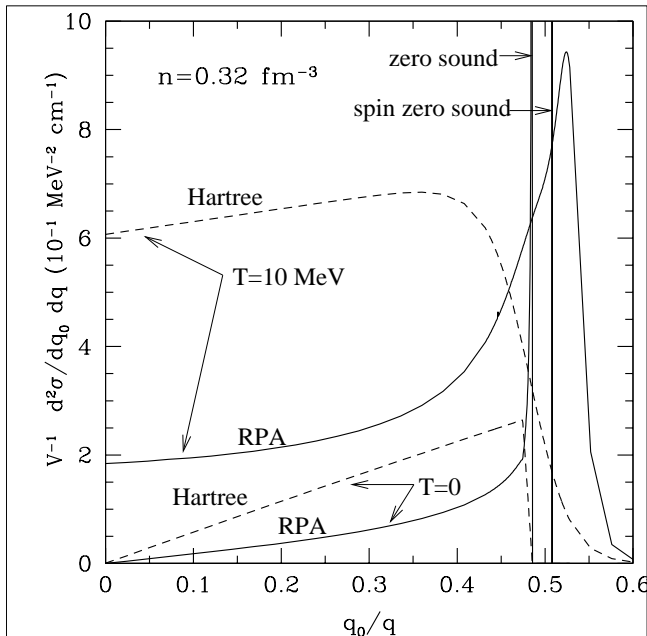


Figure 6. Neutrino scattering cross section as function of energy transfer q_0 in pure neutron matter for momentum transfer $q = 10$ MeV and neutrino energy $E_\nu = 50$ MeV. (from [49])

particles remaining. Depending on the value of S_b , the nuclei produced are in the iron group or, at higher entropies, can have mass numbers $A = 80 - 100$. These nuclei then become the seeds and, together with the remaining neutrons, undergo an r-process [57]. In this model a successful r-process depends mainly on four parameters: the entropy per baryon S_b , the dynamical timescale, the mass loss rate and the electron-to-baryon ratio Y_e . All parameters depend on the neutrino luminosity and are determined mostly by ν_e and $\bar{\nu}_e$ absorption on free nucleons. During a supernova explosion these parameters vary and the r-process in the hot neutrino bubble becomes a dynamical and time-dependent scenario. Woosley et al. [54] have calculated the r-process abundance for this site, adopting the parameters as given by Wilson's successful supernova model (e.g. Fig. 4). The final abundances obtained after integration over the duration of the r-process in the hot neutrino bubble (several seconds) are shown in Fig. 7, showing quite satisfying agreement between calculation and observation.

Neutrino-induced reactions can be important during and even after the r-process. In the conventional picture [57] the nuclei are basically in $(n, \gamma)/(\gamma, n)$ equilibrium during the r-process. The r-process path is mainly determined by neutron separation energies and the timescale is essentially set by the β -decays of the waiting-point nuclei at the magic neutron numbers $N = 50, 82$ and 126 . However, in the presence of a strong neutrino flux, ν_e -induced charged-current reactions on the waiting-point nuclei might actually compete

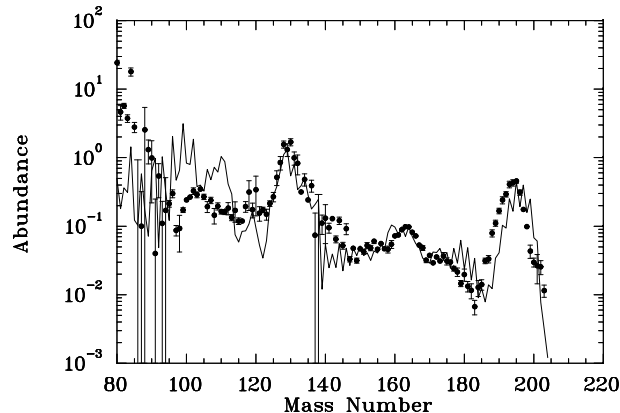


Figure 7. R-process abundances in the hot neutrino bubble model compared to observation (from [54])

with β -decays and speed-up the passage through the bottle-necks at the magic neutron numbers [59]. It is found [59] that, for typical neutrino luminosities and spectra, ν_e -capture rates are of order 5 s^{-1} and thus can be faster than competing β -decays for the slowest waiting-point nuclei. Of course, quantitative conclusions can only be drawn from detailed numerical simulations of the r-process. A first step towards this goal has recently been made by Meyer et al. [58].

It is usually assumed that the r-process drops out of $(n, \gamma)/(\gamma, n)$ equilibrium in a sharp freeze-out. The very neutron-rich matter, assembled during the r-process, then decays back to the valley of stability by a sequence of β -decays. However, in the neutrino-driven wind scenario the r-process matter will still be exposed to rather strong neutrino fluxes, even after freeze-out. By both ν_e -induced charged-current and ν_x -induced neutral-current reactions, neutrinos can inelastically interact with r-process nuclei. In these processes the final nucleus will be in an excited state and most likely decay by the emission of one or several neutrons. Thus, this *post-processing* of r-process matter after freeze-out might effect the final r-process abundance. The neutrino post-processing effects depend on the neutrino-induced neutron knock-out cross sections, which Qian *et al.* [59] have calculated based on the continuum random phase approximation and the statistical model, and on the total neutrino fluence through the r-process ejecta following freeze-out.

The dominant features of the observed r-process abundance distribution are the peaks at $A \sim 130$ and 195 , corresponding to the progenitor nuclei with $N = 82$ and 126 closed neutron shells. Haxton et al. [59] find that 8 nuclei, lying in the window $A = 124 - 126$ and $183-187$, are unusually sensitive to neutrino post-processing [60]. These nuclei sit in the valleys immediately below the abundance peaks which can be readily filled by spallation off the abundant isotopes in the peaks. To avoid overproduction of the nuclei in these abundance windows one is able to place upper bounds on the fluence ($\mathcal{F} \leq 0.045$ at $A \sim 130$ and ≤ 0.030 at $A \sim 195$, respectively). Furthermore, it turns out that

the observed abundance of the nuclei in the two abundance windows can be consistently reproduced by the same fluence parameter (for an example see Fig. 8). This might be taken as evidence suggesting that the r-process does occur in an intense neutrino fluence, and thus that the interior region of a type II supernova is the site of the r-process.

We like to stress that the neutrino-induced knock-out liberates about 3-5 neutrons from nuclei in the abundance peaks around $A = 130$ and 195. Thus this process cannot be able to fill the well-developed abundance trough at $A \approx 115$ [61] where r-process simulations with conventional mass formulae strongly underestimate the observed abundances. This discrepancy might point to interesting nuclear structure effects in very neutron-rich nuclei, related to shell quenching far from stability [62].

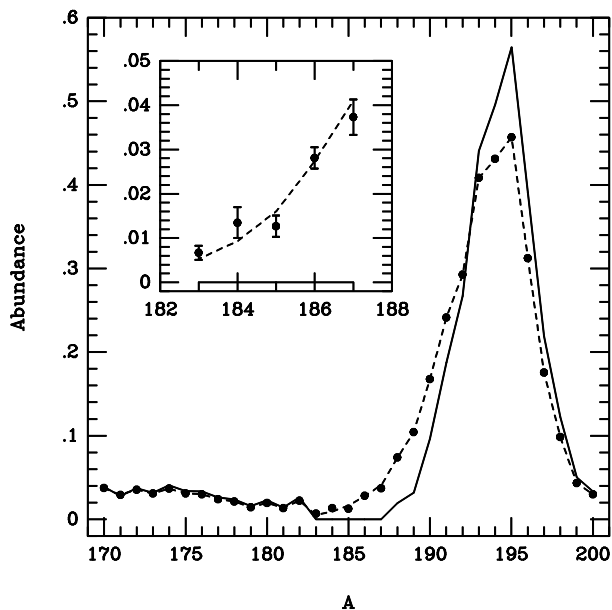


Figure 8. Effect of postprocessing by neutrino-induced reactions on the r-process abundance. The unprocessed distribution (solid line) is compared with the distribution after postprocessing (dashed line). A constant fluence of $\mathcal{F} = 0.015$ has been assumed which provides a best fit to the observed abundances for $A = 183 - 87$ (see inset). The observed abundances are plotted as filled circles with error bars. (from [59])

The open question currently is what kind of superpositions of entropies the supernova neutrino-driven wind environment really provides. In the supernova model used by Woosley et al [54] entropies upto $S_b = 300$ have been reached, but other models suggest that S_b is a factor of 3-5 smaller (e.g. [55]). To understand the importance of the entropy, one has to consider that the production of seed nuclei has to go through the bottleneck of the 3-body reaction $\alpha + \alpha + n \rightarrow {}^9\text{Be}$ at the start. Due to the low Q-value of this reaction ($Q = 1.57$ MeV), a large entropy (or high photon number) drives this reaction in

equilibrium to the left, ensuring a rather small amount of ${}^9\text{Be}$. Since all ${}^9\text{Be}$ is basically transformed into seed nuclei, a high entropy results in a small amount of seed nuclei and a large neutron-to-seed ratio n/s [63].

As a simple measure for a successful r-process one has to require the presence of enough neutrons to synthesize nuclei in the r-process peak around $A = 200$ beginning from the seed nuclei ($A \leq 100$). Thus, the neutron-to-seed ratio n/s has to reach at least 100 for a successful r-process. Systematic studies by Hoffmann and collaborators [64] and Freiburghaus *et al.* [56] have shown that a successful r-process requires either large entropies at the Y_e values currently obtained in supernova models, or smaller values for Y_e .

6. Testing the supernova models

Supernova SN1987A in the Large Magellanic Cloud confirmed the fundamental ideas of the theoretical picture of type II supernovae. Due to models, the supernova produces an appreciable amount of ${}^{56,57}\text{Ni}$ which decays within a few days to ${}^{56,57}\text{Co}$ (the supernova is not transparent at these early times and these decays are not observed). The observed lightcurve of SN1987A then followed the decay of ${}^{56}\text{Co}$ (with a half-life of 77 days) and later ${}^{57}\text{Co}$ (271 days), exactly as expected [65,66], and a total amount of 0.075 solar masses of ${}^{56}\text{Co}$ could be implied. Now the lightcurve is powered by the decay of ${}^{44}\text{Ti}$ with a half-life of 60 years. The special role, played by the observation of γ lines originated from the decay of ${}^{44}\text{Ti}$, for the detection of past supernovae will be reviewed below. However, before we like to briefly discuss the detection of supernova neutrinos.

6.1. Observation of ν_μ and ν_τ neutrinos in Superkamiokande

In what is considered the birth of neutrino astrophysics and the most outstanding single observation from supernova SN1987A, 19 neutrinos have been detected by the Kamiokande [67] and IMB [68] water Čerenkov detectors. Although being only a few events, these neutrinos give evidence for the collapse of the iron core of the evolved massive progenitor to a neutron star, and even allow to derive constraints on neutrino properties. It is generally assumed that these events originated from the $\bar{\nu}_e + p \rightarrow n + e^+$ reaction in water. The detection of ν_e and ν_x neutrinos via the $\nu + e \rightarrow \nu' + e'$ scattering or the ${}^{16}\text{O}(\nu_e, e^-){}^{16}\text{F}$ reaction was strongly suppressed by the small effective cross sections of these processes, although the ν_e induced signal can in principle be separated by its angular distribution [69]. Thus, SN1987A did not allow for a detailed test of the neutrino distribution and, in particular, it gave no information about ν_x neutrinos, which as we discussed above, should decouple deepest in the star. The observability of supernova neutrinos has significantly improved since the Superkamiokande (SK) detector, with a threshold of 5 MeV, is operational [70]. If we were lucky enough and a supernova occurs in our galaxy in the near future, this detector is indeed able to supply the desired information about the neutrino distributions and temperature hierarchy, and can therefore test the change of neutrino opacities due to the nuclear medium.

Recently a new signal for the observation of ν_x neutrinos in water Čerenkov detectors has been proposed [71]. Schematically the detection scheme works as follows. Supernova ν_x neutrinos, with average energies of ≈ 25 MeV, will predominantly excite 1^- and 2^- giant resonances in ${}^{16}\text{O}$ via the ${}^{16}\text{O}(\nu_x, \nu'_x){}^{16}\text{O}^*$ neutral current reaction [72]. These resonances

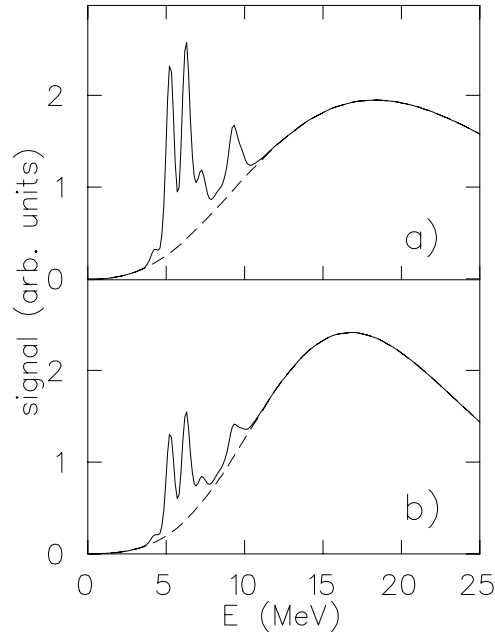


Figure 9. Signal expected from supernova neutrinos in a water Cerenkov detector calculated for two different types of neutrino distributions (without chemical potential (above) and with chemical potential $\mu = 3T$ and temperatures $T = 6.26$ MeV (for ν_x) and $T = 4$ MeV (for $\bar{\nu}_e$)). The bulk of the signal stems from $\bar{\nu}_e$ neutrinos reacting with protons, while the ν_x neutrinos induce the superimposed signal at energies $E = 5 - 10$ MeV. (from [71])

are above the particle thresholds and will mainly decay by proton and neutron emission. Although these decays will be dominantly to the ground states of ^{15}N and ^{15}O , respectively, some of them will go to excited states in these nuclei. If these excited states are below the particle thresholds in ^{15}N ($E^* < 10.2$ MeV) or ^{15}O ($E^* < 7.3$ MeV), they will decay by γ emission. As the first excited states in both nuclei ($E^* = 5.27$ MeV in ^{15}N and $E^* = 5.18$ MeV in ^{15}O) are at energies larger than the SK detection threshold, all of the excited states in ^{15}N and ^{15}O below the respective particle thresholds will emit photons which can be observed in SK.

Based on a calculation which combines the Continuum RPA with the statistical model [71], Superkamiokande is expected to observe about 360 γ events in the energy window $E = 5 - 10$ MeV, induced by ν_x neutrinos (with a FD distribution of $T = 8$ MeV), for a supernova going off at 10 kpc ($\approx 3 \cdot 10^4$ lightyears or the distance to the galactic center). This is to be compared with a smooth background of about 270 positron events from the $\bar{\nu}_e + p \rightarrow n + e^+$ reaction in the same energy window (see Fig. 9). The number of events produced by supernova ν_x neutrinos via the scheme proposed here is larger than the total number of events expected from ν_x -electron scattering (about 80 events [70]). More importantly, the γ signal can be unambiguously identified from the observed spectrum in

the SK detector, in contrast to the more difficult identification from ν_x -electron scattering. The proposed scheme will also increase the neutral current signal for supernova neutrinos in the heavy water detector SNO, but it is weaker than the one stemming from dissociation of the deuteron.

6.2. Observation of supernova γ rays

In recent years gamma-ray astronomy has grown into a fascinating tool to study past nucleosynthesis [73]. The first observation of the 1.809 MeV γ -rays stemming from the decay of ^{26}Al [74] has boosted the field, and in the meantime an all-sky image of current nucleosynthesis in our galaxy has been derived from the observations of COMPTEL [75]. Noting that γ rays penetrate the interstellar medium without significant interaction, the mean life time of ^{26}Al ($\approx 10^6$ years) is, however, too long to assign the observed γ rays to a specific supernova event. This is different for the 1.157 MeV γ rays observed in 1994 in the Cas A supernova remnant [76] stemming from the ^{44}Ti decay chain.

Supernova models predict a small amount of ^{44}Ti produced in the α -rich freeze-out in the core. With a half-life of 60 years [78,79], ^{44}Ti decays to ^{44}Sc which then decays fast to an excited state in ^{44}Ca whose deexcitation produces the observed 1.157 MeV γ rays. As the CAS A supernova remnant is young and close (the event happened between 1668-1680 at a distance of 3.4 kpc), COMPTEL was able to measure the flux of the line rather precisely [77] and, knowing the half-life of ^{44}Ti , an ejected amount of about $2.4 \cdot 10^{-4}$ solar masses in ^{44}Ti could be deduced.

Note, however, that not all of the core matter is ejected, as matter inside the mass cut is accreted onto the compact remnant of the supernova. The mass cut, i.e. the coordinate which separates ejected and accreted matter, is largely unknown and is usually heuristically determined in model calculations. In this way, the determination of the ^{44}Ti yields allow to fix the mass cut coordinate in the models, which then predict the ejected amount of other radioactive material. For example, CAS A should then have ejected about 0.05 solar masses of ^{56}Ni , making it a rather bright and easily visible supernova. However, the absence of historical records suggest a rather large visual extinction at the time of the explosion, possibly caused by extra material distributed closely to CAS A, as suggested by ROSAT studies of the X-ray scattering halo of the supernova remnant [80].

It is interesting to note that the ejected mass of ^{44}Ti inferred from SN1987A (a type II event) and from CAS A (a type Ib event) is rather similar. Nevertheless a direct observation of the 1.157 MeV γ rays from SN1987A has not been successful yet. Improved data are expected from the next generation of γ ray observatories like INTEGRAL to be launched in 2001. One of the goals will be to determine the Galactic supernova rate.

7. Explosive hydrogen burning

Wallace and Woosley have pointed out that hydrogen can also be burnt explosively in a variety of high-temperature, high-density environments such as type II supernovae shock waves and binary systems involving accretion onto white dwarfs (leading to nova explosions) or neutron stars (x-ray bursts). At temperatures higher than those for ‘normal’ hydrostatic CNO-cycle hydrogen burning, extended hydrogen burning involving other cycles of nuclei such as NeNaMg, MgAlSi or SiPS can occur at greatly accelerated rates [83]. For temperatures ranging from a few times 10^8 K to above 10^9 K, and densities

ranging from 10^3 g/cm³ to 10^6 g/cm³, hydrogen burning can transmute nuclei from the CNO region to much heavier nuclei during explosive time scales (1-100 seconds); the higher temperature and density, the further up the chart of nuclides the rp-process (short for rapid proton capture) can progress. The rp-process proceeds by radiative proton captures and β^+ decays along a path close to the proton dripline; a few (α, γ) and (α, p) reactions will occur as well.

Under nova conditions, temperatures and densities of $4 \cdot 10^8$ K and 10^4 g/cm³ are reached. Under these conditions the (experimentally unknown) $^{15}\text{O}(\alpha, \gamma)^{19}\text{Ne}$ rate is expected to be too slow to connect the CNO cycle with the higher hydrogen cycles; a mass flow to heavier nuclides will only occur if neon is already available in the accreting white dwarf (e.g. ONeMg white dwarf). In this case mass flow up to the sulfur region is possible in novae [84]. If the accreting compact object is a neutron star, nuclear burning is ignited at high densities ($\approx 10^6$ g/cm³) in the accreted envelope via the pp-chain, the hot CNO cycle and the triple- α process. The released energy triggers a thermonuclear runaway; the peak temperatures of $2 \cdot 10^9$ K, which can be reached before the degeneracy is lifted, are high enough to trigger an rp-process. Depending on the time scale available, simulations find matter flow up to ^{56}Ni or even further up to ^{96}Cd [85] (see Fig. 10).

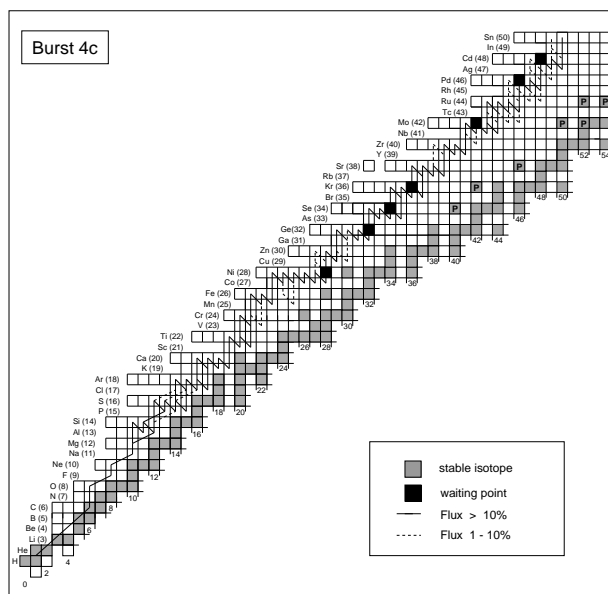


Figure 10. Reaction flow pattern in explosive hydrogen burning under x-ray burst conditions (courtesy of H. Schatz, [81]).

Similar to the r-process, studies of the rp-process require the knowledge of masses, lifetimes and capture cross sections for unstable (proton-rich) nuclei. Many accelerators, such as the NSCL at Michigan State University, the TRIUMF accelerator in Vancouver,

Louvain-La-Neuve in Belgium, GSI in Darmstadt and the RIKEN accelerator in Japan, have contributed much to the determination of these quantities. It should be noted that, unlike the r-process, the small reaction Q-values (often less than 2 MeV) do not permit the application of statistical model cross sections; the relevant capture cross sections have to be determined experimentally. Thus, a decisive boost to simulations of the rp-process is expected from the radioactive ion-beam facilities currently under construction in America, Europe and Japan.

It is a pleasure to thank R. Diehl, H.-T. Janka, G. Martinez-Pinedo and H. Schatz to provide material used in this manuscript. Many fruitful discussions with F.-K. Thielemann are gratefully acknowledged. My own research has benefitted from collaboration with D.J. Dean, W.C. Haxton, E. Kolbe, S.E. Koonin, G. Martinez-Pinedo, Y.-Z. Qian, P.B. Radha, M.R. Strayer, and P. Vogel. The research has been partly supported by a grant of the Danish Research Council.

REFERENCES

1. W.A. Fowler, *Rev. Mod. Phys.* **56** (1984) 149.
2. NuPECC report on *Nuclear and Particle Astrophysics*, F.-K. Thielemann (convener) et al., (1998).
3. E.M. Burbidge, G.R. Burbidge, W.A. Fowler and F. Hoyle, *Rev. Mod. Phys.* **29** (1957) 547.
4. A.G.W. Cameron, Chalk River Report CRL-41 (1957).
5. B.E.J. Pagel and G. Trautvaisiene, *MNRAS* **276** (1995) 505; **288** (1997) 108.
6. F. Timmes, S.E. Woosley and T.A. Weaver, *Ap.J. Suppl.* **98** (1995) 617.
7. T. Tsujimoto, K. Nomoto, Y. Yoshii, M. Hashimoto and F.-K. Thielemann, *MN* **277** (1995) 945.
8. L. Buchmann, R.E. Azuma, C.A. Barnes, J. Humblet and K. Langanke, *Phys. Rev.* **C54** (1996) 393 and references therein.
9. E. Anders and N. Grevesse, *Geochim. Cosmochim. Acta* **53** (1989) 197.
10. S.E. Woosley, D. Hartmann, R.D. Hoffman and W.C. Haxton, *Astrophys. J.* **356** (1990) 272
11. H.A. Bethe, G.E. Brown, J. Applegate and J.M. Lattimer, *Nucl. Phys.* **A324** (1979) 487
12. H.A. Bethe, *Rev. Mod. Phys.* **62** (1990) 801
13. G.M. Fuller, W.A. Fowler and M.J. Newman, *ApJS* **42** (1980) 447; **48** (1982) 279; *ApJ* **252** (1982) 715; **293** (1985) 1
14. M. B. Aufderheide, I. Fushiki, S. E. Woosley, and D. H. Hartmann, *Astrophys. J. Suppl.* **91** (1994) 389
15. A.L. Williams *et al.*, *Phys. Rev.* **C51** (1995) 1144
16. W.P. Alford *et al.*, *Nucl. Phys.* **A514** (1990) 49
17. M.C. Vetterli *et al.*, *Phys. Rev.* **C40** (1989) 559
18. S. El-Kateb *et al.*, *Phys. Rev.* **C49** (1994) 3129
19. T. Rönquist *et al.*, *Nucl. Phys.* **A563** (1993) 225

20. M.B. Aufderheide, Nucl. Phys. **A526** (1991) 161
21. M.B. Aufderheide, S.D. Bloom, D.A. Ressler and G.J. Mathews, Phys. Rev. **C47** (1993) 2961
22. M.B. Aufderheide, S.D. Bloom, D.A. Ressler and G.J. Mathews, Phys. Rev. **C48** (1993) 1677
23. E. Caurier, G. Martinez-Pinedo, F. Nowacki and A. Poves, to be published
24. C. W. Johnson, S. E. Koonin, G. H. Lang, and W. E. Ormand, Phys. Rev. Lett. **69**, 3157 (1992).
25. S. E. Koonin, D. J. Dean, and K. Langanke, Phys. Rep. **278**, 1 (1997).
26. D.J. Dean, K. Langanke, L. Chatterjee, P.B. Radha, and M.R. Strayer, Phys. Rev. **C58** (1998) 536.
27. K. Langanke and G. Martinez Pinedo, Phys. Lett. **B436** (1998) 19; preprint nucl-th/9809082; in preparation; G. Martinez Pinedo, K. Langanke and D.J. Dean, preprint nucl-th/9811095
28. D. Rudolph et al., submitted to Physical Review Letters
29. G. Martinez-Pinedo, K. Langanke, E. Caurier, F. Nowacki and A.P. Zuker, to be published
30. K. Langanke, D. J. Dean, P. B. Radha, Y. Alhassid, and S. E. Koonin, Phys. Rev. **C 52**, 718 (1995).
31. B.A Brown and B.H. Wildenthal, Ann. Rev. Nucl. Part. Sci. **38**, 29 (1988).
32. G. Martinez-Pinedo, A. Poves, E. Caurier, and A. P. Zuker, Phys. Rev. **C 53**, R2602 (1996).
33. M.B. Aufderheide, I. Fushiki, G.M. Fuller and T.A. Weaver, ApJ. **424** (1994) 257.
34. S.A. Colgate, in *Supernovae*, Jerusalem School, World Scientific (1990)
35. P.Goldreich and S.V. Weber, Ap.J. **238** (1980) 991.
36. A. Burrows, Ann. Rev. Nucl. Sci. **40** (1990) 181.
37. A. Burrows, Ap.J. **334** (1988) 891.
38. J.R. Wilson, in *Numerical Astrophysics*, ed. by J.M. Centrella, J.M. LeBlanc and R.L. Bowers, (Jones and Bartlett, Boston, 1985) p. 422
39. Y. Fukuda *et al.*, Phys. Rev. Lett. **81** (1998) 1562.
40. A. Burrows and B.A. Fryxell, Science **258** (1992) 430.
41. E. Müller and H.-T. Janka, Astron. Astrophys. **317** (1997) 140.
42. E. Müller, in *Nuclear Astrophysics*, eds. M. Buballa, W. Nörenberg, J. Wambach and A. Wirzba (GSI publication, 1998)
43. H.-T. Janka, private communication
44. M. Herant, W. Benz and S.A. Colgate, Ap.J. **395** (1992) 642.
45. A. Burrows, J. Hayes and B.A. Fryxell, Ap.J. **450** (1995) 830.
46. H.-T. Janka and E. Müller, Astron. Astrophys. **306** (1996) 167.
47. T. Shimizu, S. Yamada and K. Sato, Ap.J. **432** (1994) L119.
48. S. Reddy, M. Prakash and J.M. Lattimer, Phys. Rev. **D58** (1998) 3009.
49. S. Reddy, J. Pons, M. Prakash and J.M. Lattimer, in *Stellar Evolution, Stellar Explosion and Galactical Chemical Evolution*, ed. A. Mezzacappa (Institute of Physics Publishing, Bristol, 1998) p. 585.
50. A. Burrows and R.F. Sawyer, Phys. Rev. **C58** (1998) 554.
51. S. Reddy, M. Prakash, J.M. Lattimer and S.A. Pons, submitted to Phys. Rev. **D**

52. A. Akma, V.R. Pandharipande and D.G. Ravenhall, Phys. Rev. C58 (1998) 1804.
53. A. Burrows and R.F. Sawyer, preprint, astro-ph/9804264.
54. S.E. Woosley, J.R. Wilson, G.J. Mathews, R.D. Hoffmann and B.S. Meyer, Ap.J. 433 (1994) 229.
55. J. Witt, H.-Th. Janka and K. Takahashi, Astron. Astrophys. **286** (1994) 841 and (1994) 857
56. F.-K. Thielemann, T. Rauscher, C. Freiburghaus, K. Nomoto, M. Hashimoto, B. Pfeiffer and K.-L. Kratz, to be published
57. J.J. Cowan, F.-K. Thielemann, J.W. Truran, Phys. Rep. **208** (1991) 267.
58. B.S. Meyer, G.C. McLaughlin and G.M. Fuller, Phys. Rev. C, in print; preprint astro-ph/9809242.
59. Y.-Z. Qian, W.C. Haxton, K. Langanke and P. Vogel, Phys. Rev. **C55** (1997) 1532
60. W.C. Haxton, K. Langanke, Y.-Z. Qian and P. Vogel, Phys. Rev. Lett. **78** (1997) 2694
61. K.-L. Kratz, J.-P. Bitouzet, F.-K. Thielemann, P. Möller and B. Pfeiffer, Astrophys. J. **402** (1993) 216
62. B. Chen, J. Dobaczewski, K.-L. Kratz, K. Langanke, B. Pfeiffer, F.-K. Thielemann, Phys. Lett. **B355** (1995) 37
63. Y.-Z. Qian and S.E. Woosley, Astrophys. J. **471** (1996) 331
64. R.D. Hofmann, S.E. Woosley and Y.-Z. Qian, ApJ 482 (1997) 951.
65. S.E. Woosley, P.A. Pinto and D.H. Hartmann, Ap.J. 346 (1989) 395.
66. D.D. Clayton and L.S. The, Ap.J. 375 (1991) 221.
67. K.S. Hirata *et al.*, Phys. Rev. Lett. **58** (1987) 1490
68. R.M. Bionta *et al.*, Phys. Rev. Lett. **58** (1987) 1494.
69. W. C. Haxton, Phys. Rev. **D36** (1987) 2283.
70. Y. Totsuka, Rep. Progr. Phys. **55** (1992) 377.
71. K. Langanke, P. Vogel and E. Kolbe, Phys. Rev. Lett. **76** (1996) 2629
72. E. Kolbe, K. Langanke, S. Krewald and F.-K. Thielemann, Nucl. Phys. A540 (1992) 599.
73. N. Prantzos and R. Diehl, Phys. Rep. 267 (1996) 1.
74. W.A. Mahoney et al., ApJ. 262 (1982) 742.
75. U. Oberlack, R. Diehl, D.H. Hartmann and M.D. Leising, in *Stellar Evolution, Stellar Explosion and Galactical Chemical Evolution*, ed. A. Mezzacappa (Institute of Physics Publishing, Bristol, 1998) p. 179.
76. A.F. Iyudin et al., Astron. Astrophys. 284 (1994) 11.
77. A.F. Iyudin et al., in *Proceedings of the 2nd INTEGRAL workshop*, eds. C. Winkler, T.J.-L. Courvoisier, P. Durouchoux, ESA SP-282 (1997) 37.
78. J. Görres et al., Phys. Rev. Lett. 80 (1998) 2554.
79. E. Norman et al., Phys. Rev. C57 (1998) 2010.
80. P. Predehl and J.H. Schmitt, Astron. Astrophys. 293 (1995) 889.
81. H. Schatz, private communication
82. R.K. Wallace and S.E. Woosley, Ap.J. Suppl. 45 (1981) 389.
83. A.E. Champagne and M. Wiescher, Ann. Rev. Nucl. Part. Sci. 42 (1992) 39.
84. L. van Woermer et al., Ap.J. 432 (1994) 326.
85. H. Schatz et al., Phys. Rep. 294 (1998) 167.